Copy 258
RM E52B21

NACA RM E52B21

6729

NACA

RESEARCH MEMORANDUM

AERODYNAMIC INTERFERENCE EFFECTS ON NORMAL AND

AXIAL FORCE COEFFICIENTS OF SEVERAL

ENGINE-STRUT-BODY CONFIGURATIONS

AT MACH NUMBERS OF 1.8 AND 2.0

By Emil J. Kremzier and Murray Dryer

Lewis Flight Propulsion Laboratory
Cleveland, Ohio

NATIONAL ADVISORY COMMITTEE
FOR AERONAUTICS
WASHINGTON
April 28, 1952

2438

NATIONAL ADVISORY COMMITTEE FOR AERONAUTICS

RESEARCH MEMORANDUM

AERODYNAMIC INTERFERENCE EFFECTS ON NORMAL AND AXIAL FORCE

COEFFICIENTS OF SEVERAL ENGINE-STRUT-BODY CONFIGURATIONS

AT MACH NUMBERS OF 1.8 AND 2.0

By Emil J. Kremzier and Murray Dryer

SUMMARY

Aerodynamic interference effects associated with a missile config-
uration, consisting of a pointed body of revolution with one or two ram-
jet engines strut-mounted in a vertical plane through the center line
of the body, were investigated for several engine locations relative to
the body and for a range of angles of attack from 0° to 10°. The inves-
tigation was conducted in the Lewis 8- by 6-foot supersonic wind tunnel
at Mach numbers of 1.8 and 2.0 and at a test Reynolds number of approxi-
mately 28×10^6 based on body length.

The experimental data indicated increases in slope of the normal
force curve with outward movement of the engines. Several of the out-
board engine positions actually resulted in normal force curve slopes
slightly in excess of the sum of the slopes of the normal force curves
of the isolated components.

Decreases in axial force occurred with inboard rearward movement
of the engines. Maximum decreases in axial forces of the order of 20
to 34 percent less than the sum of the axial forces of the isolated com-
ponents were noted for the various configurations.

Validity of the theoretical prediction of normal and axial force
interference effects was limited to the approximate determination of the
trend of these effects with changes in engine location; magnitudes of
theoretical and experimental values showed agreement in only a few
isolated cases. Body viscous cross-flow separation at higher angles of
attack affected the flow field of the upper engine to such an extent
that theoretical normal force evaluation was not feasible.

Comparison of lift-drag ratios of various configurations in combina-
tion with a hypothetical wing of given lift-drag ratio indicated that the
trend of lift-drag ratio of the complete configuration with varying engine
position was governed by configuration drag whereas the effect of config-
uration lift was not noticeable. The trend of lift-drag ratios for the

various configurations was not necessarily the same as that for the various combinations with a wing; this difference indicated the necessity of considering a complete aircraft in the evaluation of lift-drag ratio.

INTRODUCTION

In the design of supersonic aircraft incorporating a nacelle-body combination, the location of the nacelle with respect to the body has an important influence on aerodynamic interference effects from the standpoint of aircraft lift and drag. Some typical transonic and high subsonic investigations of configurations with nacelle-like bodies of revolution mounted in various positions on sweptback wings are reported in references 1 and 2. The results of these investigations show favorable drag interference effects at zero lift for certain nacelle locations. As part of a general program at the NACA Lewis laboratory to investigate aerodynamic interference effects of nacelle-body combinations at supersonic Mach numbers, reference 3 presents experimental data for various combinations of one and two nacelles (hereinafter called engines) mounted on struts in the vertical plane through the center line of a body. This report is an extension of reference 3 and includes an analysis of the data and a comparison with theory where possible. A brief analysis of the effect of engine location on configuration lift-drag ratio is also included.

Configuration normal and axial force coefficients were determined for various engine locations at Mach numbers of 1.8 and 2.0 through a range of angles of attack from 0° to 10°. The tests were conducted in the Lewis 8- by 6-foot supersonic wind tunnel at a Reynolds number of approximately 28×10^6 based on body length.

APPARATUS AND PROCEDURE

A sketch of the model which consisted of the NACA RM-10 body with two ram-jet engines mounted symmetrically in a vertical plane through the center line of the body is shown in figure 1. Engine location with respect to the body was variable, and the upper or lower engine was separately removable. Force and pressure instrumentation were incorporated as described in reference 3.

Lift and drag coefficients of reference 3 were reduced to normal and axial force coefficients for purposes of analysis. All force coefficients were obtained from forebody forces only; that is, the base pressures were corrected to free-stream static pressure, and the internal aerodynamic forces were excluded from the balance readings. Normal

2438

forces resulting from the turning of the internal stream tube in the vicinity of the engine inlet are included in the normal force coefficients, inasmuch as they are essentially independent of engine internal flow conditions for supercritical flow.

RESULTS AND DISCUSSION

Characteristics of Isolated Components

In order to evaluate the effects of aerodynamic interference on the body-engine configuration, the characteristics of the isolated components must be considered.

Isolated body. - Normal and axial force coefficients for the isolated body have been plotted as a function of angle of attack for Mach numbers of 1.8 and 2.0 in figure 2. Theoretical normal force coefficients were calculated by the method of reference 4. Theoretical axial force coefficients at zero angle of attack were obtained from the sum of the pressure drag given by linearized potential theory and the friction drag calculated from the equation for turbulent incompressible flow over a smooth flat plate (reference 5). The axial friction force coefficient was assumed constant with angle of attack, and the axial pressure force coefficient was assumed to vary in accordance with linearized potential theory. As observed from the figure, reasonably good agreement is noted between experiment and theory. Furthermore, these data, which were presented in terms of lift and drag coefficient curves in reference 3, substantiate reasonably well the results presented in references 6 and 7 for previous investigations of the RM-10 body.

Isolated engine. - Normal and axial force coefficients are presented in figure 3 for the same range of variables covered with the isolated body. Theoretical curves for the external normal force coefficient were obtained by the method of reference 4, the equations of which were modified to apply to an open-nosed body. Internal normal force was evaluated from the momentum change in a full-inlet stream tube in turning from the free-stream to the axial direction of the engine. The theoretical axial force coefficients at zero angle of attack were obtained from the sum of the theoretical friction drag (based on two-dimensional compressible flow theory of reference 8) and the theoretical pressure drag calculated from the curves presented in reference 9. Friction forces were then assumed constant with angle of attack and pressure forces were again assumed to vary in accordance with linearized potential theory. A comparison between the experimental and the theoretical curves indicates reasonably good agreement.

Normal force curves for both the isolated body and the isolated engine exhibit continuously increasing slopes with increasing angle of

attack. The variation of axial force coefficient with angle of attack
is quite small for both body and engine.

Characteristics of Representative Configurations

The trends of the curves for normal and axial force coefficients as
a function of angle of attack are similar for most configurations inves-
tigated. These trends are illustrated in figure 4 for a representative
configuration (B-2B) at Mach numbers of 1.8 and 2.0. As noted for the
isolated body and isolated engine, the normal force curve slope exhibits
a gradual continuous increase with increasing angle of attack, whereas
the variation in axial force throughout the angle of attack range is
quite small. Several of the configurations (upper engine) have slight
decreases in their normal force curve slopes at the higher angles of
attack as a direct result of the loss in normal force of the upper engine
as it becomes immersed in the body wake. A more detailed discussion of
these phenomena will be presented later.

Interference Effects

Experimental normal force. - In order that some concept as to the
magnitude and trend of the effects of aerodynamic interference on the
normal force curve slope may be acquired, a normal force interference
factor i_N is defined as

$$i_N = \frac{\left[\dfrac{dC_N}{d\alpha}\right]_c - \left[\left(\dfrac{dC_N}{d\alpha}\right)_b + \left(\dfrac{dC_N}{d\alpha}\right)_e\right]}{\left[\left(\dfrac{dC_N}{d\alpha}\right)_b + \left(\dfrac{dC_N}{d\alpha}\right)_e\right]}$$

(All symbols are defined in appendix A.) A negative interference factor
therefore indicates that the slope of the curve for the complete config-
uration is less than the sum of the slopes of its individual components.
For convenience, interference factors i_N were evaluated at angles of
attack of 2° and 8° so that representative interference effects in the
lower $(0^\circ < \alpha < 4^\circ)$ and higher $(6^\circ < \alpha < 10^\circ)$ ranges of angles of
attack could be compared. The use of normal force curve slopes in the
evaluation of i_N gives qualitative comparisons of normal force inter-
ference effects; however, actual values of the normal force coefficient
at angles of attack of 2° and 8° are tabulated in table I, together with
the corresponding slope of the curve at these angles for the various
configurations investigated. In calculating the interference factor,
normal force effects due to the presence of the engine mounting struts
were neglected, inasmuch as these effects are believed to be quite small.

2438

The solid lines of figures 5 and 6 are experimental contour plots
of lines of constant normal force interference factor at angles of
attack of 2° and 8°, respectively, for the range of engine locations
investigated. Coordinates of the curves represent the position of inter-
section of the engine and strut center lines in the vertical plane
relative to the body.

In general, the interference factor varied from some negative value
to a slight positive value with outward movement of the engines and, in the
absence of the strut, would return to a zero value when the respective
body and engine flow fields become sufficiently separated that no inter-
action occurred, but the range of engine locations investigated was gen-
erally insufficient to verify this condition. A general trend of less
negative interference factor with rearward movement of the engines was
also noted on most of the plots, although this variation was small com-
pared with that observed with outward movement of the engines. No
significant Mach number effects were noted.

Variation of $(i_N)_{\alpha=2°}$ with lateral movement of the engines was
greater for twin-engine configurations than that for upper- or lower-
engine configurations (fig. 5). For example, $(i_N)_{\alpha=2°}$ for twin-engine
configurations at a Mach number of 2.0 varied from -0.25 for inboard
engine positions to +0.05 for outboard positions; whereas normal
force curve slopes for inboard engine positions of single-engine con-
figurations exhibited a maximum reduction of 10 to 15 percent of that
for the sum of the slopes of the isolated components. If the negative
interference factors of lower- and upper-engine configurations are
added algebraically, approximate results for twin-engine configura-
tions are obtained; this result indicates negligible engine-engine
interference effects. Interference of body wake on the engines or
engine wake on the body is small at low angles of attack, as
evidenced by the quantitative similarity of the family of curves in
figures 5(b) and 5(c) for lower- and upper-engine configurations,
respectively.

Contours of the normal force interference factor $(i_N)_{\alpha=8°}$ are
shown in figure 6. A comparison of the slopes of the contours for the
twin-engine and upper-engine configurations at angles of attack of 2°
(figs. 5(a) and 5(c)) and 8° (figs. 6(a) and 6(c)) shows a reversal in the
trend of i_N with longitudinal engine movement. The variation of
$(i_N)_{\alpha=8°}$ with lateral engine movement is also much greater than that of
$(i_N)_{\alpha=2°}$ for these configurations. This reversal in trend of the
$(i_N)_{\alpha=8°}$ curves, together with the rather severe reduction in normal
force curve slope for inboard engine positions, is believed to be caused
by the immersion of the upper engine in the cross-flow vortex field of
the body, the formation of which occurs at the higher angles of attack
as discussed in references 10 and 11. The energy losses associated with
this vortex field cause reductions in the normal force contribution of

the upper engine. The magnitude of this reduction will, of course, be
dependent upon the extent of immersion of the engine in the vortex field.
On the other hand, $(i_N)_{\alpha=8^o}$ contours for the lower-engine configura-
tions (fig. 6(b)) show variations that are comparable $((i_N)_{\alpha=8^o} = -0.10$
for inboard forward engine positions) to those noted at an angle of
attack of 2° (fig. 5(b)); similar negligible engine wake effects are thus
indicated. For example, the configuration with the upper engine mounted
in the rearmost inboard position has a normal force curve slope about
50 percent of that of the sum of the slopes of the individual components,
whereas the analogous lower-engine position shows no interference. It is
concluded that even for high angles of attack of the order of 8°, lower-
engine configurations will experience normal force interference effects
due primarily to downwash or upwash rather than to viscous effects exper-
ienced by upper- and twin-engine configurations.

Theoretical normal force. - An attempt was made to predict theoreti-
cally the slopes of the normal force curves for the various configurations.
Accordingly, interference lift curve slopes for the various body-engine
combinations were calculated by the method presented in reference 12 and
outlined in appendix B.

In order to compare the results of this theoretical treatment of the
lift curve slope with experimental values, theoretical lift interference
factors were calculated in the same manner as the normal force interfer-
ence factor $(i_N)_{\alpha=2^o}$ for the various configurations. The theoretical
lifts (considered now as normal force at the low angles of attack) per
unit angle of attack for the separate components were calculated by means
of slender-body theory. The results are shown as dashed line contours
in figure 5 for twin-, lower-, and upper-engine configurations, respec-
tively, at Mach numbers of 1.8 and 2.0.

Theoretical and experimental curves of figure 5 both show the same
qualitative trends and magnitudes. The magnitudes, however, are seldom
exactly the same. The theoretical treatment may therefore be used as a
guide for predicting the trend of the normal force interference effects
as well as approximate magnitudes for various engine locations. When the
distance between body and engine center lines is of the same order of
magnitude as the body or engine diameter, the slender-body approximation
is less valid and results in misleading interference factors. This
phenomenon is especially marked in the vicinity of forward engine loca-
tions (fig. 5). In any event, these discrepancies indicate the need for
further refinements in the theoretical treatment.

At the higher angles of attack where linearized theory does not
account for the viscous cross forces on the body and one or both engines,
an average value of the body upwash calculated by the method of refer-
ence 12 was arbitrarily used. This upwash provided a constant cross flow

2438

along the length of the engine and, together with the method outlined
in reference 4, a viscous cross force due to this interference upwash
was calculated and presented in the same manner as the preceding inter-
ference factor. The lift curve slopes of the body and engine alone were
also adjusted to account for the viscous cross forces. The results are
also presented as interference factor contours for lower-engine config-
urations and appear as dashed lines in figure 6(b). When compared with
experimental results, this technique is satisfactory only for lower-
engine locations in the vicinity of the forward engine position.
Because of the small variation in normal force interference factor with
engine position, viscous interference effects are of secondary impor-
tance for lower-engine configurations at the higher angles of attack.
The upwash, which is of primary importance, produces a small amount of
favorable experimental interference for rearward engine locations
(fig. 6(b)) which is not predicted by this method. The theoretical
results obtained for twin- and upper-engine configurations are similar
to those obtained for lower-engine configurations but are not presented
because of the poor agreement obtained as a result of large adverse
effects of the vortex street on the upper engine which are not predicted
by any presently available theory.

Experimental axial force. - The variation in axial force coefficient
with angle of attack was quite small for all configurations investigated,
as previously illustrated in figure 4. Consequently, only zero angle of
attack data will be used in discussing axial force interference effects.
Accordingly, an axial force interference factor is defined as

$$i_A = \frac{C_{A,c} - \left(C_{A,b} + C_{A,e} + C_{A,s}\right)}{C_{A,b} + C_{A,e} + C_{A,s}}$$

A negative value of i_A indicates that the axial force of the complete
configuration is less than the sum of the axial forces of the isolated
components. Strut axial force coefficient was obtained by multiplying
the exposed strut length by the axial force coefficient per unit length
based on maximum body diameter. The drag of the body with two struts
for two different strut lengths as presented in reference 3 was used to
determine the strut drag per unit length $(C_{A,s})$ at zero angle of attack
(same as axial force). Values of $C_{A,s}$ of 0.00450 per inch at M_0 of
1.8 and 0.00464 per inch at M_0 of 2.0 were obtained.

Contour plots of experimental axial force interference factor are
presented in figure 7 (solid lines). Single-engine configuration plots
were obtained from average faired values of axial force coefficients of
corresponding upper- and lower-engine configurations since their axial
forces are actually the same. In general, the interference factor varies

from approximately zero for the foremost position of the engines to some negative value for the rearmost inboard engine position. Figure 7 indicates that these negative values of i_A result in reductions of axial force coefficient of from 20 to 34 percent of that obtained from the sum of the axial forces of the individual components. For twin-engine configurations, i_A decreases with increasing strut length to some minimum value and then increases again for forward engine positions. Thus, it is possible to have two different strut lengths exhibiting the same value of i_A in one of these given forward longitudinal engine positions.

Theoretical axial force. - Theoretical interaction drag for the various configurations investigated may be determined by the method of reference 13. This interaction drag evaluated in the form of an axial force interference factor contour plot for single- and twin-engine configurations at Mach numbers of 1.8 and 2.0 is presented in figure 7 (dashed lines). A considerable difference in magnitude between experiment and theory is observed particularly for the inboard engine positions. For example, an experimental drag decrease of about 25 percent is noted for configuration C-1B (fig. 7(a), $M_0 = 1.8$), whereas theory predicts a value of about 15 percent. These differences probably arise largely from inaccuracies associated with slender-body theory when the distance between center lines of interacting bodies becomes small in comparison with the body diameters. Furthermore, the body interference drag that results from the flow field generated by the engine due to presence of the body was neglected. The radial velocity component, which was not considered in the theory, may also have some effect on the drag when the engines are mounted close to the body. Strut interaction drag is another factor that was not considered in the theoretical calculations, although the contribution of the struts is probably negligible for the shorter strut lengths. It is evident, therefore, that a more exact theoretical treatment is desirable. Despite the differences in magnitude noted between the experimental and theoretical values of i_A, the theoretical values indicate the greatest decrease in drag with the engines in the rearmost inboard position. This decrease has also been noted experimentally and a value less than the sum of the axial forces of the isolated components results directly from location of the engines in a region of favorable buoyancy.

Base pressure. - Body base-pressure coefficient as a function of engine-body center-line distance for the various configurations investigated is presented in figure 8 for zero angle of attack and Mach numbers of 1.8 and 2.0. The dashed lines give values of base-pressure coefficient for the isolated body.

Inconsistancies are noted in the trends of the coefficients with increasing strut length as shown in figure 8 for the various configurations. However, the base pressures generally are more negative for the body-engine configurations at zero angle of attack than for the isolated

2438

body. Reference 6 also shows decreases in base pressure for the RM-10 body with the additional stabilizing fins, indicating that the addition of external appendages causes increases in base drag for all cases cited.

Effect of Engine Location on Lift-Drag Ratio

In order to evaluate the significance of the trend of configuration lift-drag ratios with engine position, comparison of the configuration lift-drag ratio $(L/D)_c$ with a composite aircraft lift-drag ratio (configuration with wing) $(L/D)_t$ will be made. Since the range of angles of attack covered in the present investigation did not permit attainment of peak configuration lift-drag ratios (reference 3), variation of $(L/D)_c$ and $(L/D)_t$ with engine movement at a fixed angle of attack will be considered.

Contour plots of lines of constant $(L/D)_c$ for various engine locations are shown in figures 9(a), 10(a), and 11(a) for twin-engine, lower-engine, and upper-engine configurations, respectively, at M_0 of 2.0 and α_c of 8°. The contours are governed by the relative variations of the lift and drag coefficients for various engine locations, and no consistent trends among the three figures are noted.

If a composite aircraft is simulated by combining the preceding configurations with a wing of given lift-drag ratio and neglecting the interference effects between the wing and the engine-body combination, the aircraft lift-drag ratio becomes

$$(L/D)_t = \frac{\dfrac{W_G}{q_0 S_m}}{(C_D)_c + \dfrac{\dfrac{W_G}{q_0 S_m} - (C_L)_c - C_T \sin \alpha}{(L/D)_w}} \qquad (1)$$

Figures 9(b), 10(b), and 11(b) present contour plots of $(L/D)_t$ utilizing a wing combined with the twin-engine, lower-engine, and upper-engine configurations, respectively. The following assumptions were made:

W_G = 50,000 pounds q_0 = 678 pounds per square foot

Altitude = 50,000 feet $(L/D)_w$ = 5.0

S_m = 27.2 feet α_c = 8°

M_0 = 2.0   NACA standard atmosphere

The value of $(L/D)_t$ for all configurations is seen to increase with rearward inboard engine movement. The decrease of configuration drag with inward, rearward positioning of the engines (reference 3) supports the trend of the $(L/D)_t$ contours. Decreases of configuration lift with inward movement of the engines oppose this trend. It may be concluded, therefore, that configuration drag governs the trend of the aircraft $(L/D)_t$, whereas configuration lift is only of secondary importance. Thus, a comparison of the configuration alone with the configuration with wing curves (figs. 9 to 11) shows that the addition of a wing may change the lift-drag ratio characteristics of engine-body combinations. In any event, the complete aircraft should be considered when an engine-body configuration is chosen as part of the aircraft.

SUMMARY OF RESULTS

Engine-strut-body configurations with the engines mounted in a vertical plane through the center line of the body were investigated in the Lewis 8- by 6-foot supersonic wind tunnel at Mach numbers of 1.8 and 2.0. The following interference effects on the aerodynamic characteristics were noted:

1. For twin-engine (above and below body) as well as single-engine (above body or below body) configurations with the engines located close to the body, the normal force curve slopes were about 10 to 25 percent less than the sum of the slopes for the individual components at $0° < \alpha < 4°$, where α is the angle of attack. As one or both engines were moved outward and rearward, this interference effect diminished to zero and then became slightly favorable. The adverse interference was greater for twin-engine configurations because of apparent additive interference from each engine. Theoretical calculations may be used as a guide for predicting the above trend of normal force curve slopes, although quantitative agreement was only fair.

2. For single-engine configurations at $6° < \alpha < 10°$ with the engines mounted under the body in forward inboard positions, normal force curve slopes were about 10 percent less than the sum of the slopes for the individual components. Rearward engine movement resulted in interference effects similar to those experienced at $0° < \alpha < 4°$, which indicated negligible viscous interference. For twin-engine and single-engine above-body configurations at $6° < \alpha < 10°$, normal force curve slopes were reduced as much as 50 percent of the sum of the slopes for the individual components for inboard engine positions because of immersion of the upper engine in the body vortex field. Outward movement of one or both engines resulted in diminishing viscous effects until negligible interference occurred.

2438

Theoretical calculations, which included a small viscous approxima-
tion, failed to predict the viscous interference for twin- and upper-
engine configurations because of the large effect of the viscous cross
flow on the upper engine. The calculation, however, partly verified the
dominant role of interference upwash for lower engine configurations.

3. Decreases in axial force coefficient for all configurations with
inboard rearward movement of the engines were noted. For the various
configurations, decreases in axial force of the order of 20 to 34 percent
less than the sum of the axial forces of the isolated components were
obtained. Theoretical calculations also indicated that the greatest
decreases in axial force were obtained with the engines in the rearmost
inboard position, although quantitative agreement between experiment
and theory was poor.

4. Calculations of lift-drag ratio of a composite aircraft utilizing
the configurations investigated indicated that configuration drag played
a dominant role in determining the magnitude of the lift-drag ratio whereas
configuration lift was only of secondary importance. Comparison of the
trend of the lift-drag ratios of the configurations with a hypothetical
wing and the lift-drag ratios of the configurations alone with varying
engine location showed that the lift-drag ratios of the configurations
alone may or may not have the same trend as the complete configurations.
The complete aircraft should thus be considered when lift-drag ratio is
evaluated.

Lewis Flight Propulsion Laboratory
     National Advisory Committee for Aeronautics
          Cleveland, Ohio

APPENDIX A

SYMBOLS

A external forebody axial force

A_{cyl} cross-sectional area of hypothetical cylinder whose volume is equal to portion of body between 1b and 2b and whose length is equal to (2b - 1b)

b local body radius

C_A axial forebody force coefficient, $A/q_0 S_m$

C_D external forebody drag coefficient, $D/q_0 S_m$

C_L lift coefficient, $L/q_0 S_m$

C_N normal force coefficient, $N/q_0 S_m$

C_{p_b} base-pressure coefficient, $(p_b - p_0)/q_0$

C_T internal thrust coefficient, $F/q_0 S_m$

D external forebody drag

F internal thrust

i_A axial force interference factor, $\dfrac{C_{A,c} - \left(C_{A,b} + C_{A,e} + C_{A,s}\right)}{C_{A,b} + C_{A,e} + C_{A,s}}$

i_N normal force interference factor, $\dfrac{\left[\dfrac{dC_N}{d\alpha}\right]_c - \left[\left(\dfrac{dC_N}{d\alpha}\right)_b + \left(\dfrac{dC_N}{d\alpha}\right)_e\right]}{\left[\left(\dfrac{dC_N}{d\alpha}\right)_b + \left(\dfrac{dC_N}{d\alpha}\right)_e\right]}$

L lift

$(L/D)_c$ lift-drag ratio of engine-body configuration

$(L/D)_t$ lift-drag ratio of combined wing and engine-body configuration

$(L/D)_w$ lift-drag ratio of wing

M_0 free-stream Mach number
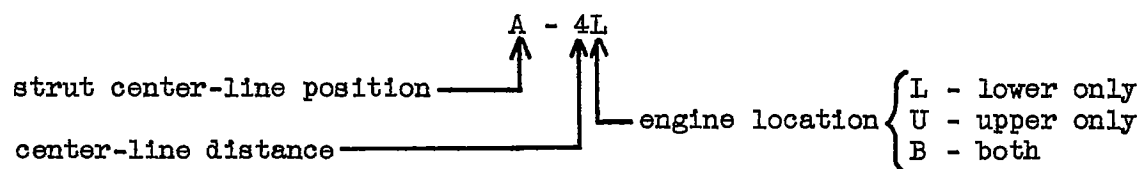
N normal force

2438

p_b base pressure

p_0 free-stream static pressure

q_0 free-stream dynamic pressure

S cross-sectional area

S_{cyl} cross-sectional area of hypothetical cylinder whose volume is equal to portion of engine between 1e and 2e and whose length is equal to (2e - 1e)

S_m maximum cross-sectional area of body

u perturbation velocity in x-direction

U free-stream velocity

w perturbation velocity in z-direction

W_G gross weight

x longitudinal distance from body nose to local station along body

z distance between body and engine center lines in the vertical plane

α angle of attack, deg

$\dfrac{dC_N}{d\alpha}$ slope of normal force curve

Subscripts:

b isolated body

B,b base of body

B,e base of engine

c body-engine configuration

e isolated engine

I,e inlet of engine

s isolated strut

1e   station at engine inlet

2e   station at intersection of engine center line and Mach line from body base

1b   station at intersection of body center line and Mach line from engine lip

2b   station at intersection of body center line and Mach line originating from corner of engine base

Configuration designation (fig. 1):

$$A - 4L$$

strut center-line position

center-line distance

engine location
{
L - lower only
U - upper only
B - both
}

APPENDIX B

EQUATIONS FOR THE DETERMINATION OF INTERFERENCE LIFT

As noted in reference 12, the following assumptions are made:

(1) The linearized differential equation of motion is assumed to apply.

(2) The lifts of the individual components are determined using slender-body theory.

(3) The upwash is constant around each body and is considered equal to its value at the center line.

(4) The contribution of the sidewash is negligible, assuming constant sidewash around each body.

Assumption (1) leads to the relation of the pressures to the upwash field by the condition of irrotationality,

$$\frac{\partial u}{\partial z} = \frac{\partial w}{\partial x} \qquad (B1)$$

From assumption (2) the lift coefficient of the body alone is the same as that resulting from an incompressible flow about an inclined body, namely,

$$C_{L,b} = 2\alpha \frac{S_{B,b}}{S_m} \qquad (B2)$$

where α is given in radians.

It should be pointed out that flow separation actually prevents the development of negative lift downstream of the body maximum cross-sectional area. Equation (B2) does not take into consideration this phenomenon and results in lift curve slopes which are about half those obtained experimentally, as noted in the following table:

α	M_0	Experiment		Theory	
		$\left(\frac{dC_N}{d\alpha}\right)_b$	$\left(\frac{dC_N}{d\alpha}\right)_e$	$\left(\frac{C_L}{\alpha}\right)_b$	$\left(\frac{C_L}{\alpha}\right)_e$
2°	1.8	0.0275	0.0280	0.0129	0.0244
2°	2.0	.0292	.0280	.0129	.0244
8°	1.8	0.0748	0.0453	0.0370	0.0327
8°	2.0	.0855	.0445	.0370	.0327

CONFIDENTIAL

If S_m were used instead of $S_{B,b}$ (assuming complete separation at S_m), better "theoretical" results would be obtained; however, it is desirable for these purposes to maintain slender-body theory in order to establish a datum upon which further approximations (for example, possible separation at S_m) may later be made.

The lift coefficient of the engine alone is similarly written as the sum of the internal and external (slender-body theory) lifts, namely,

$$C_{L,e} = 2\alpha \left(\frac{S_{B,e} + S_{I,e}}{S_m} \right) \tag{B3}$$

When the engine is located within the flow field of the body, the upwash due to the body and felt by the engine may be taken as a first approximation along the center line of the engine according to assumption (3). The resulting total external lift coefficient for the engine is then

$$\left(C_{L,e} \right)_{external} = 2\alpha \left(\frac{w_{B,e}}{U\alpha} + 1 \right) \frac{S_{B,e}}{S_m} \tag{B4}$$

The internal lift coefficient (assuming supercritical flow through the inlet) from momentum considerations is

$$\left(C_{L,e} \right)_{internal} = 2\alpha \left(\frac{w_{I,e}}{U\alpha} + 1 \right) \frac{S_{I,e}}{S_m} \tag{B5}$$

Since each engine is immersed in an upwash field which varies laterally, a further correction is made to account for the resulting buoyancy effects. As shown in reference 12, the resulting buoyant lift coefficient for the engine is

$$\left(C_{L,e} \right)_{buoyant} = 2\alpha \left[\frac{w_{1e}}{U\alpha} - \frac{w_{2e}}{U\alpha} \right] \frac{S_{cyl}}{S_m} \tag{B6}$$

Similarly, the buoyant lift coefficient for the body due to the upwash generated by the engine is

$$\left(C_{L,b} \right)_{buoyant} = 2\alpha \left[\frac{w_{1b}}{U\alpha} - \frac{w_{2b}}{U\alpha} \right] \frac{A_{cyl}}{S_m} \tag{B7}$$

Aside from the buoyant forces considered previously, no consideration is made regarding the lift of the body that results from the upwash generated by the engine due to the presence of the body.

CONFIDENTIAL

REFERENCES

1. Silvers, H. Norman, King, Thomas, J., Jr., and Pasteur, Thomas B., Jr.: Investigation of the Effect of a Nacelle at Various Chordwise and Vertical Positions on the Aerodynamic Characteristics at High Subsonic Speeds of a 45° Sweptback Wing With and Without a Fuselage. NACA RM L51H16, 1951.

2. Pepper, William B., Jr., and Hoffman, Sherwood: Comparison of Zero-Lift Drags Determined by Flight Tests at Transonic Speeds of Symmetrically Mounted Nacelles in Various Chordwise Positions at the Wing Tip of a 45° Sweptback Wing and Body Combination. NACA RM L51F13, 1951.

3. Madden, Robert T., and Kremzier, Emil J.: Data Presentation of Force Characteristics of Several Engine-Strut-Body Configurations at Mach Numbers of 1.8 and 2.0. NACA RM E51E29, 1951.

4. Allen, H. Julian: Estimation of the Forces and Moments Acting on Inclined Bodies of Revolution of High Fineness Ratio. NACA RM A9I26, 1949.

5. von Kármán, Th.: On Laminar and Turbulent Friction. NACA TM 1092, 1946.

6. Esenwein, Fred T., Obery, Leonard J., and Schueller, Carl F.: Aerodynamic Characteristics of NACA RM-10 Missile in 8- by 6-Foot Supersonic Wind Tunnel at Mach Numbers from 1.49 to 1.98. II - Presentation and Analysis of Force Measurements. NACA RM E50D28, 1950.

7. Perkins, Edward W., Gowen, Forrest E., and Jorgensen, Leland H.: Aerodynamic Characteristics of the NACA RM-10 Research Missile in the Ames 1- by 3-Foot Supersonic Wind Tunnel No. 2 - Pressure and Force Measurements at Mach Numbers of 1.52 and 1.98. NACA RM A51G13, 1951.

8. de Kármán, Th.: The Problem of Resistance in Compressible Fluids. Quinto Convegno "Volta", Reale Accademia d'Italia (Roma), Sett. 30-Ott. 6, 1935, pp. 3-57.

9. Jack, John R.: Theoretical Wave Drags and Pressure Distributions for Axially Symmetric Open-Nose Bodies. NACA TN 2115, 1950.

10. Luidens, Roger W., and Simon, Paul C.: Aerodynamic Characteristics of NACA RM-10 Missile in 8- by 6-Foot Supersonic Wind Tunnel at Mach Numbers of 1.49 to 1.98. I - Presentation and Analysis of Pressure Measurements (Stabilizing Fins Removed). NACA RM E50D10, 1950.
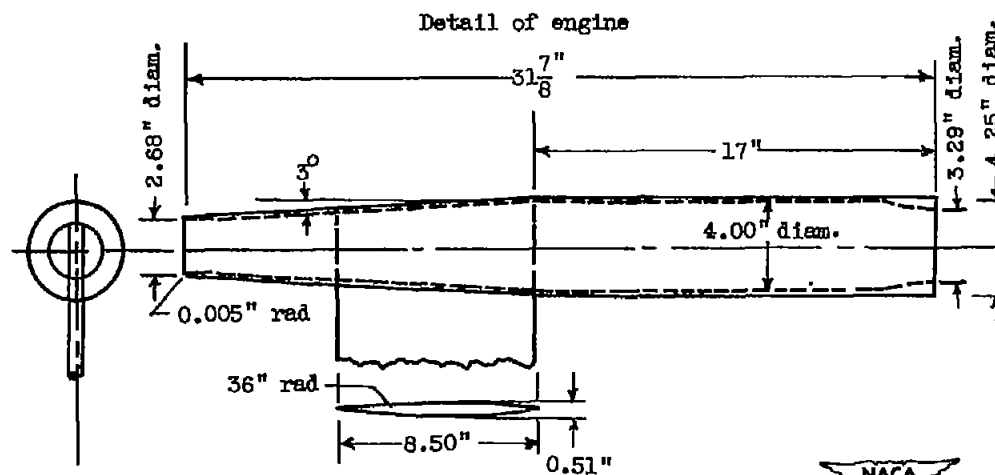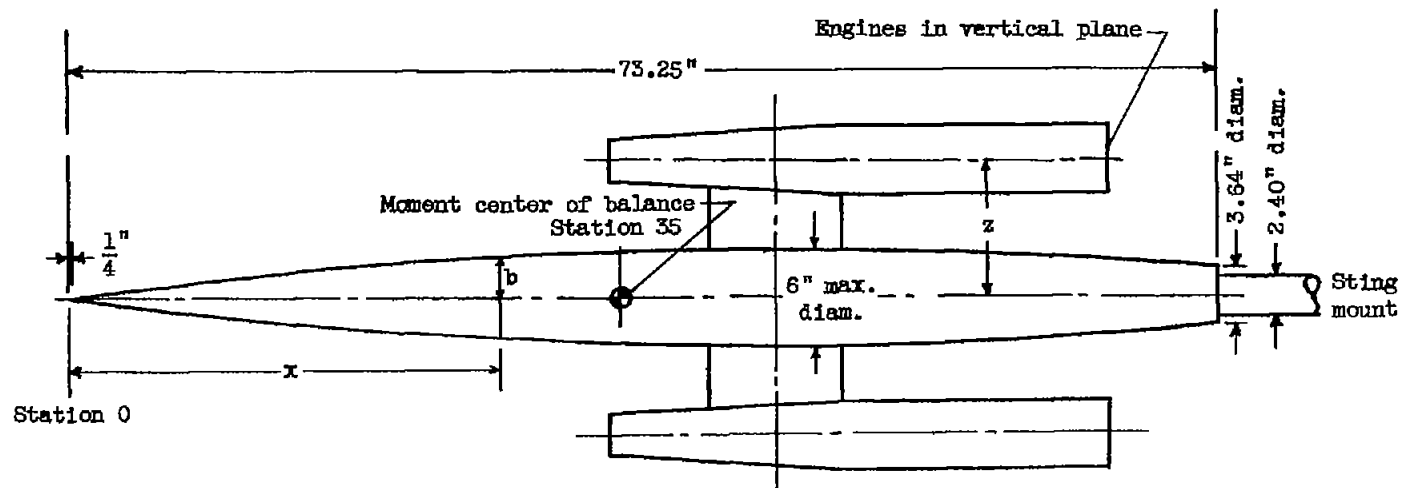
NACA RM E52B21

11. Allen, H. Julian, and Perkins, Edward W.: Characteristics of Flow Over Inclined Bodies of Revolution. NACA RM A50L07, 1951.

12. Moskowitz, Barry: Approximate Theory for Calculation of Lift of Bodies, Afterbodies, and Combinations of Bodies. NACA TN 2669, 1952.

13. Friedman, Morris D.: Arrangement of Bodies of Revolution in Supersonic Flow to Reduce Wave Drag. NACA RM A51I20, 1951.

2438

TABLE I - SUMMARY OF EXPERIMENTAL FORCE CHARACTERISTICS FOR VARIOUS CONFIGURATIONS

Configu-ration	Mach number, M_0											
	1.8						2.0					
	Angle of attack, α (deg)											
	0	2	8	2	8	0	0	2	8	2	8	0
	Normal force coefficient C_N			Slope of normal force curve $\frac{dC_N}{d\alpha}$		Axial force coefficient C_A	Normal force coefficient C_N			Slope of normal force curve $\frac{dC_N}{d\alpha}$		Axial force coefficient C_A
Body	0	0.049	0.322	0.0275	0.0748	0.113	0	0.047	0.350	0.0292	0.0855	0.113
Engine	0	.057	.269	.0280	.0453	.039	0	.063	.287	.0280	.0445	.035
A-1B	0	.140	.593	.0619	.0986	.208	0	.136	.619	.0644	.1114	.185
A-2B	0	.120	.622	.0604	.1334	.197	0	.130	.670	.0652	.1519	.176
A-3B	0	.117	.692	.0678	.1536	.219	0	.138	.761	.0761	.1689	.191
A-4B	0	.152	.765	.0772	.1576	.242	0	.176	.807	.0824	.1865	.224
B-1B	0	.143	.602	.0627	.0921	.160	0	.126	.639	.0624	.1017	.143
B-2B	0	.133	.686	.0685	.1227	.170	0	.132	.721	.0699	.1386	.151
B-3B	0	.129	.741	.0713	.1628	.207	0	.145	.822	.0793	.1778	.175
B-4B	0	.170	.826	.0834	.1671	.230	0	.177	.884	.0907	.1780	.215
C-1B	0	.123	.566	.0625	.0857	.149	0	.132	.603	.0684	.0999	.126
C-2B	0	.134	.679	.0672	.1148	.165	0	.140	.732	.0730	.1314	.137
C-3B	0	.150	.789	.0760	.1627	.185	0	.162	.884	.0822	.1712	.157
C-4B	0	.147	.836	.0821	.1621	.210	0	.164	.891	.0906	.1682	.188
A-1L	0.017	0.110	0.513	0.0485	0.1027	0.147	0.020	0.118	0.535	0.0509	0.1121	0.134
A-2L	.017	.109	.537	.0499	.1114	.152	.032	.127	.580	.0518	.1220	.145
A-3L	.034	.129	.561	.0509	.1127	.168	.036	.141	.611	.0543	.1229	.145
A-4L	.021	.125	.578	.0533	.1151	.181	.024	.122	.619	.0570	.1236	.168
B-1L	.065	.161	.602	.0505	.1163	.142	.074	.165	.635	.0511	.1261	.128
B-2L	.057	.162	.612	.0526	.1187	.145	.062	.171	.661	.0570	.1270	.128
B-3L	.042	.145	.607	.0549	.1217	.155	.052	.156	.655	.0568	.1294	.140
B-4L	.043	.150	.632	.0589	.1202	.163	.043	.160	.668	.0588	.1287	.164
C-1L	.013	.106	.544	.0503	.1202	.135	.020	.122	.608	.0551	.1316	.113
C-2L	.008	.111	.586	.0519	.1284	.130	.016	.127	.649	.0596	.1345	.113
C-3L	.021	.120	.615	.0560	.1265	.155	.040	.151	.691	.0619	.1346	.134
C-4L	.039	.153	.650	.0601	.1216	.162	.049	.167	.704	.0632	.1304	.130
A-1U	-0.032	0.055	0.403	0.0456	0.0817	0.148	-0.032	0.049	0.438	0.0475	0.0927	0.133
A-2U	-.025	.066	.465	.0471	.1059	.160	-.044	.055	.488	.0500	.1210	.133
A-3U	-.046	.054	.482	.0506	.1207	.165	-.044	.060	.523	.0530	.1354	.140
A-4U	-.025	.077	.513	.0522	.1221	.178	-.027	.070	.544	.0546	.1313	.158
B-1U	-.053	.035	.391	.0480	.0641	.130	-.064	.034	.418	.0484	.0701	.113
B-2U	-.058	.029	.450	.0488	.0968	.150	-.067	.023	.488	.0529	.1050	.125
B-3U	-.063	.041	.497	.0525	.1233	.160	-.064	.036	.534	.0551	.1364	.130
B-4U	-.047	.059	.518	.0545	.1232	.170	-.056	.057	.545	.0579	.1315	.140
C-1U	-.017	.076	.387	.0483	.0502	.128	-.020	.077	.413	.0509	.0545	.100
C-2U	-.012	.082	.492	.0513	.0748	.128	-.024	.080	.520	.0545	.0808	.110
C-3U	-.036	.068	.522	.0549	.1213	.147	-.055	.065	.559	.0615	.1282	.130
C-4U	-.043	.068	.535	.0576	.1213	.163	-.057	.065	.570	.0618	.1286	.130

NACA

Figure 1. - Engine-body configuration.

Engines in vertical plane

73.25"

3.64" diam.

2.40" diam.

Moment center of balance
Station 35

z

b

6" max.
diam.

$\frac{1}{4}$"

Sting
mount

x

Station 0

Detail of engine

Body defined by equation:

$$b = \frac{x}{15}\left[2 - \frac{x}{45}\right]$$

$$0 \leq x \leq 73.25$$

2.68" diam.

$31\frac{7}{8}$"

3.29" diam.

4.25" diam.

17"

4.00" diam.

3°

0.005" rad

36" rad

8.50"

0.51"

Strut center- line position	x (in.)
A	45
B	57
C	67.5

Center-line distance	z (in.)
1	5.12
2	6.38
3	8.50
4	10.62

2438
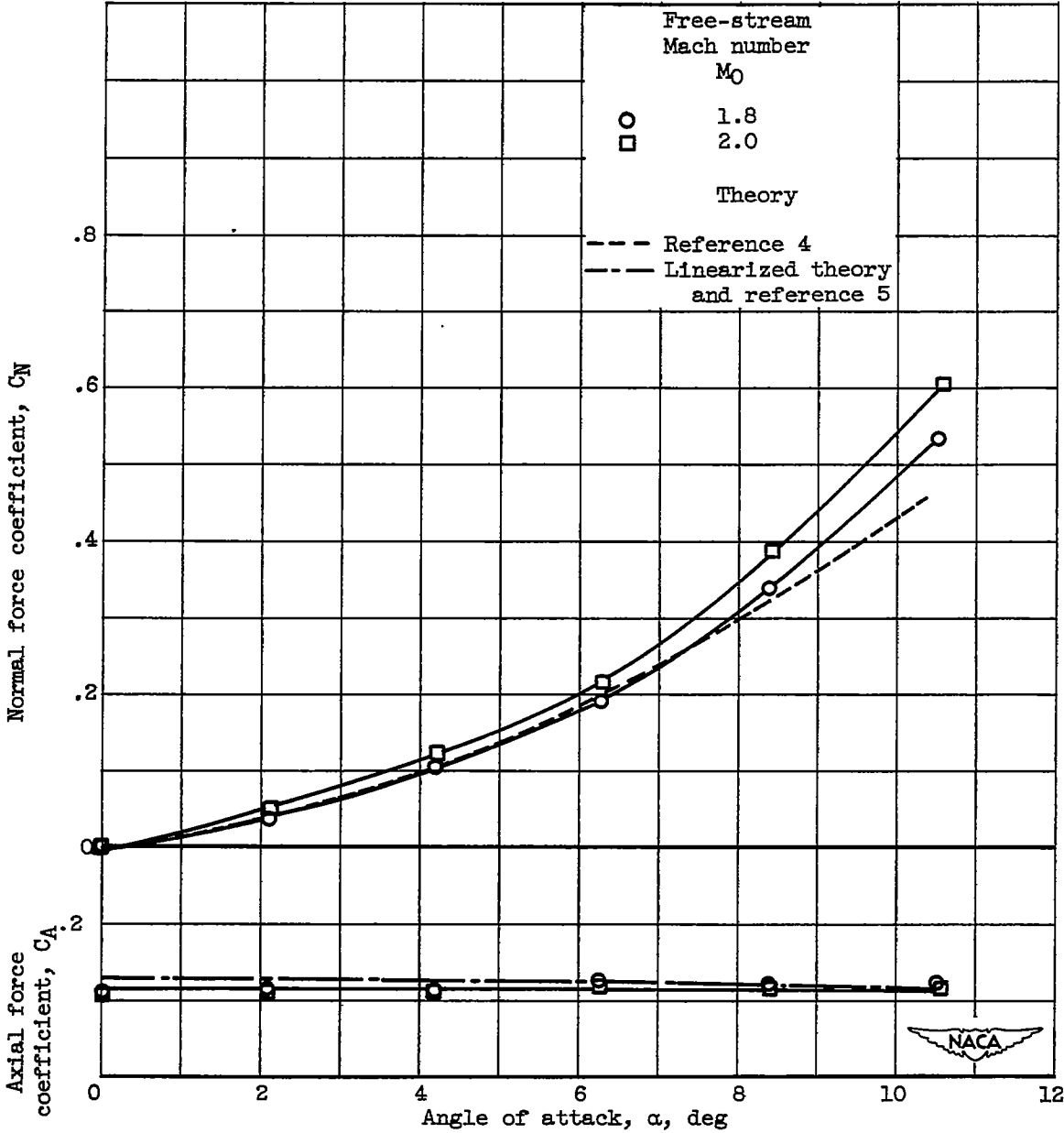
Figure 2. - Characteristics of isolated body.
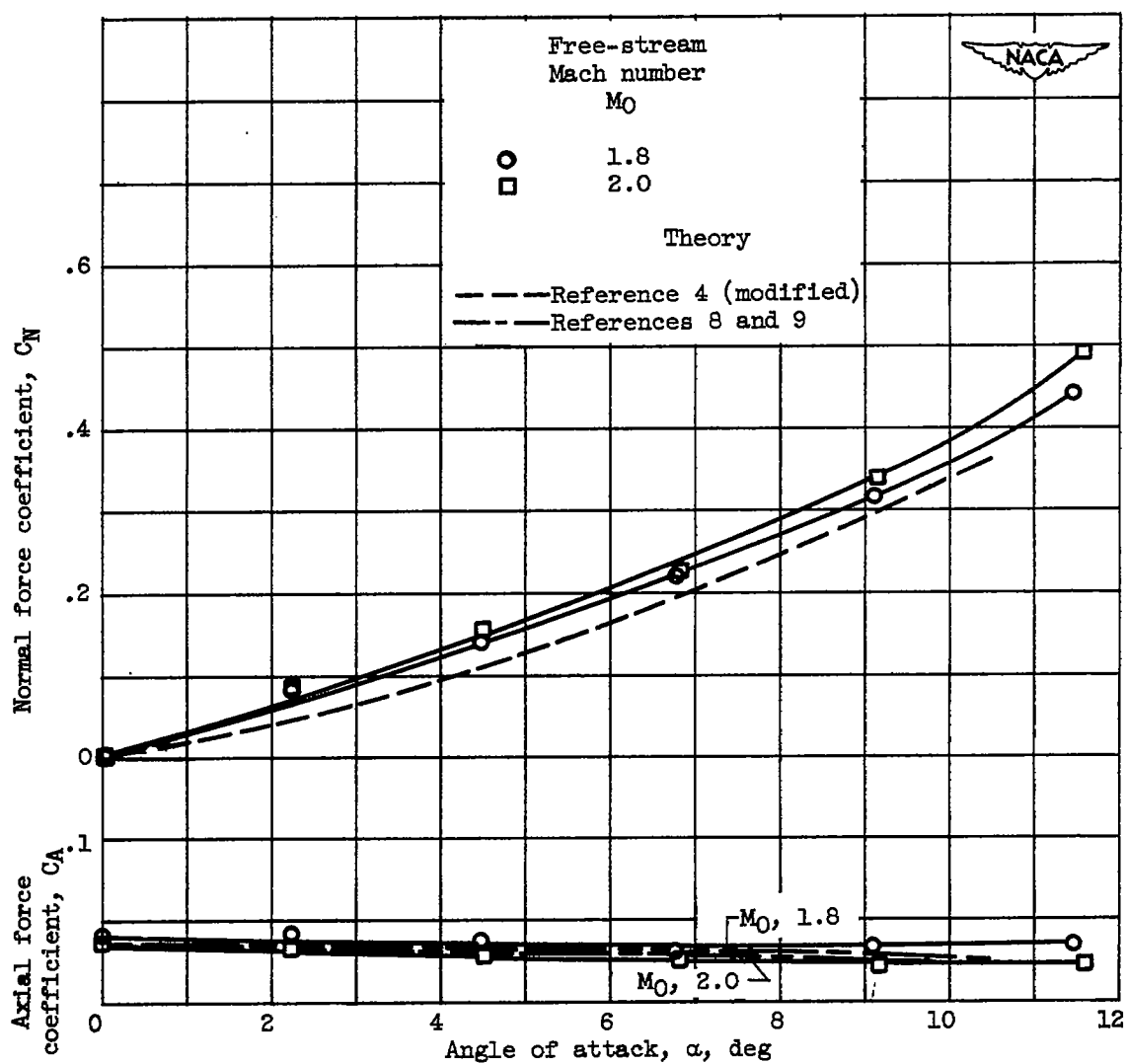
Figure 3. - Characteristics of isolated engine coefficients based on body geometry.

2438
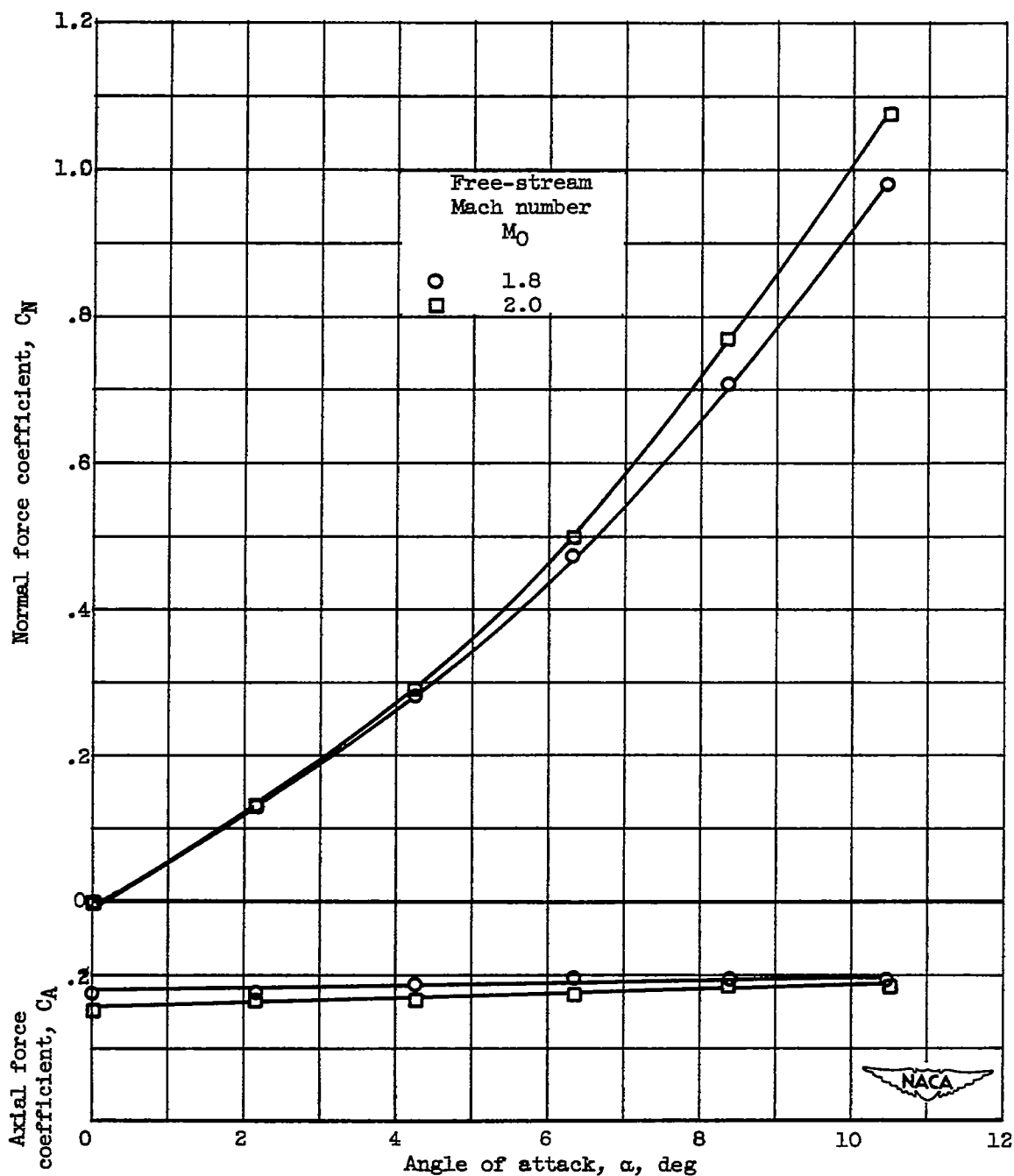
Figure 4. - Characteristics of representative configuration (B-2B).

CONFIDENTIAL
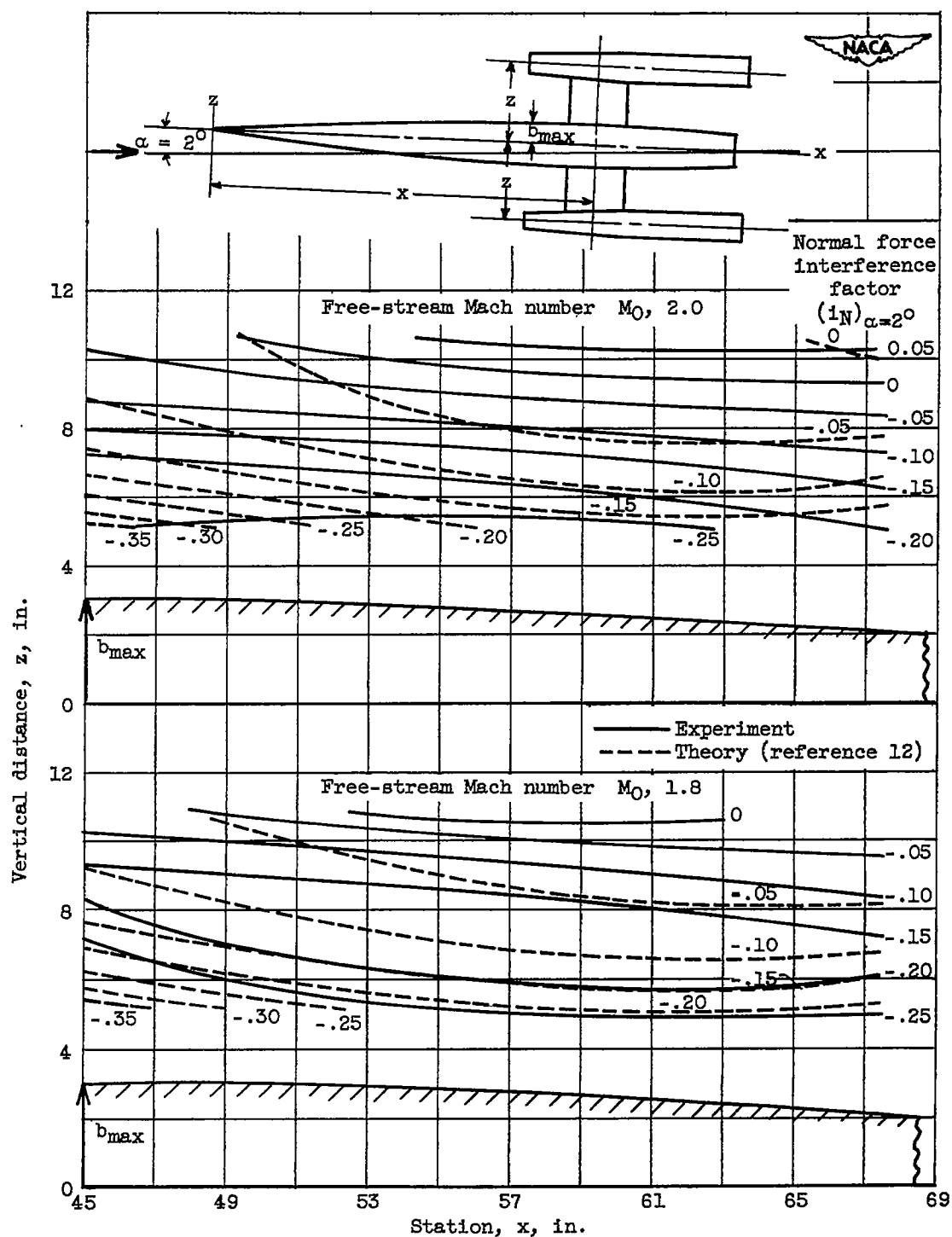
(a) Twin-engine configurations.

Figure 5. - Contours of normal force interference factor. Angle of attack, 2°.

CONFIDENTIAL

4G₁

2438
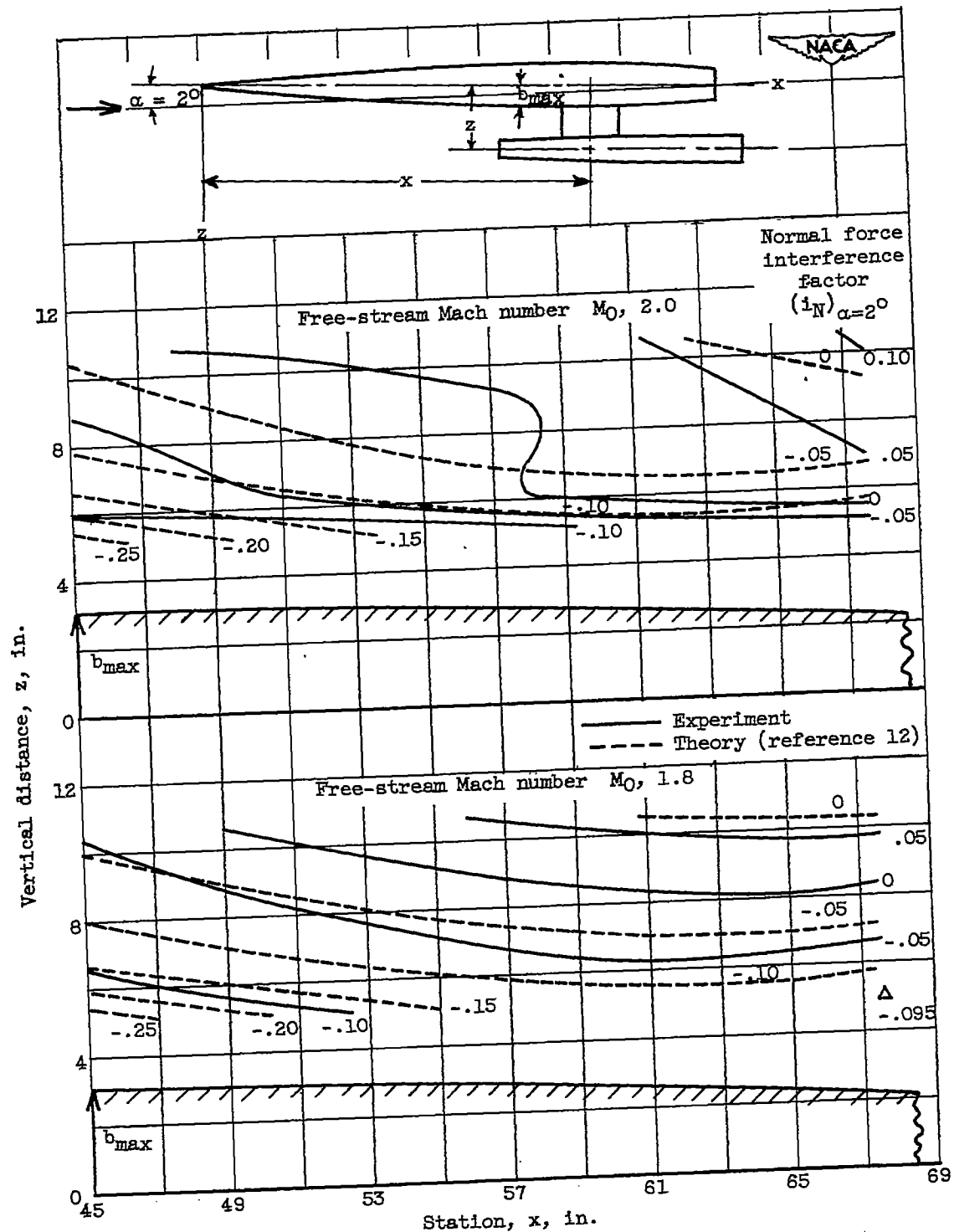
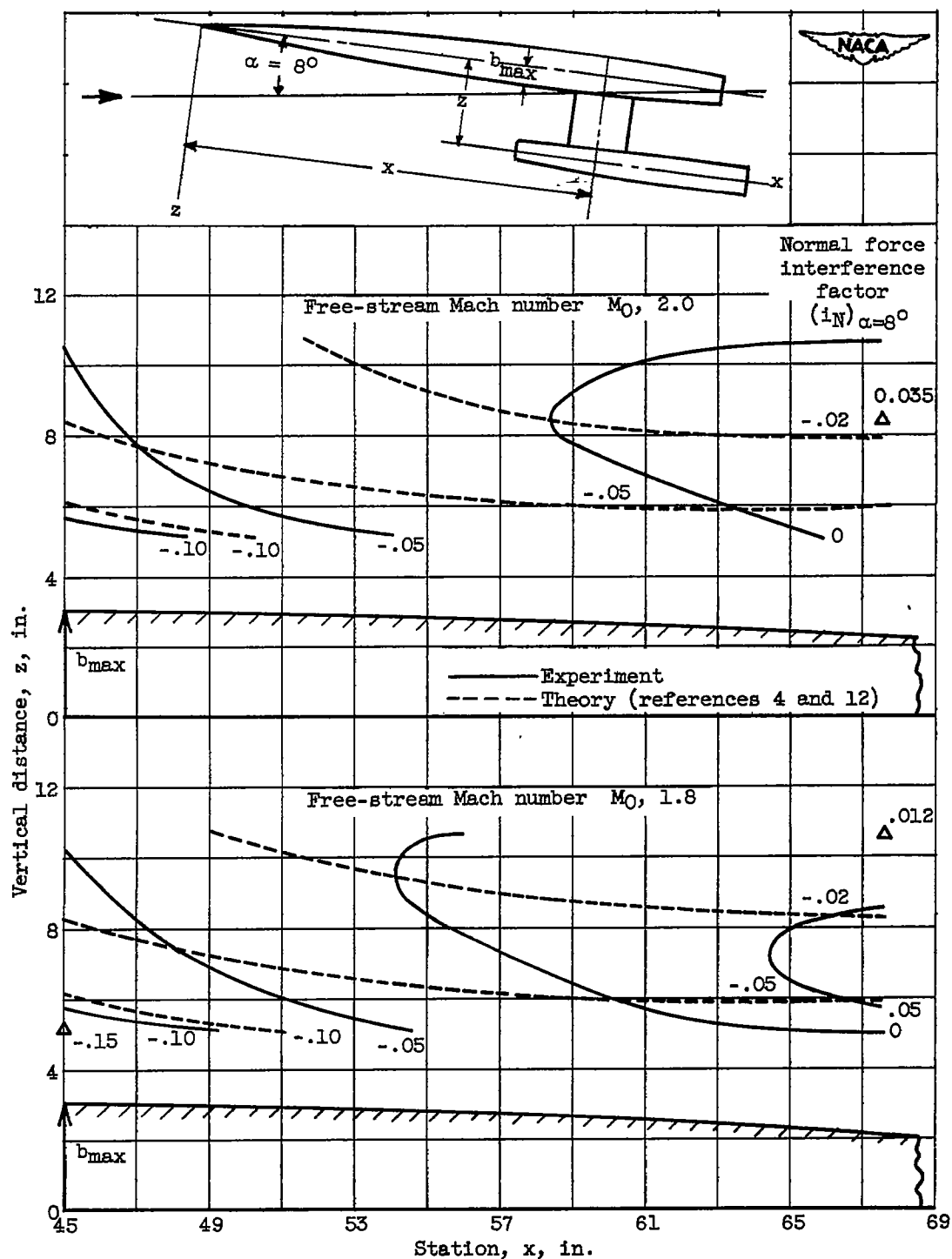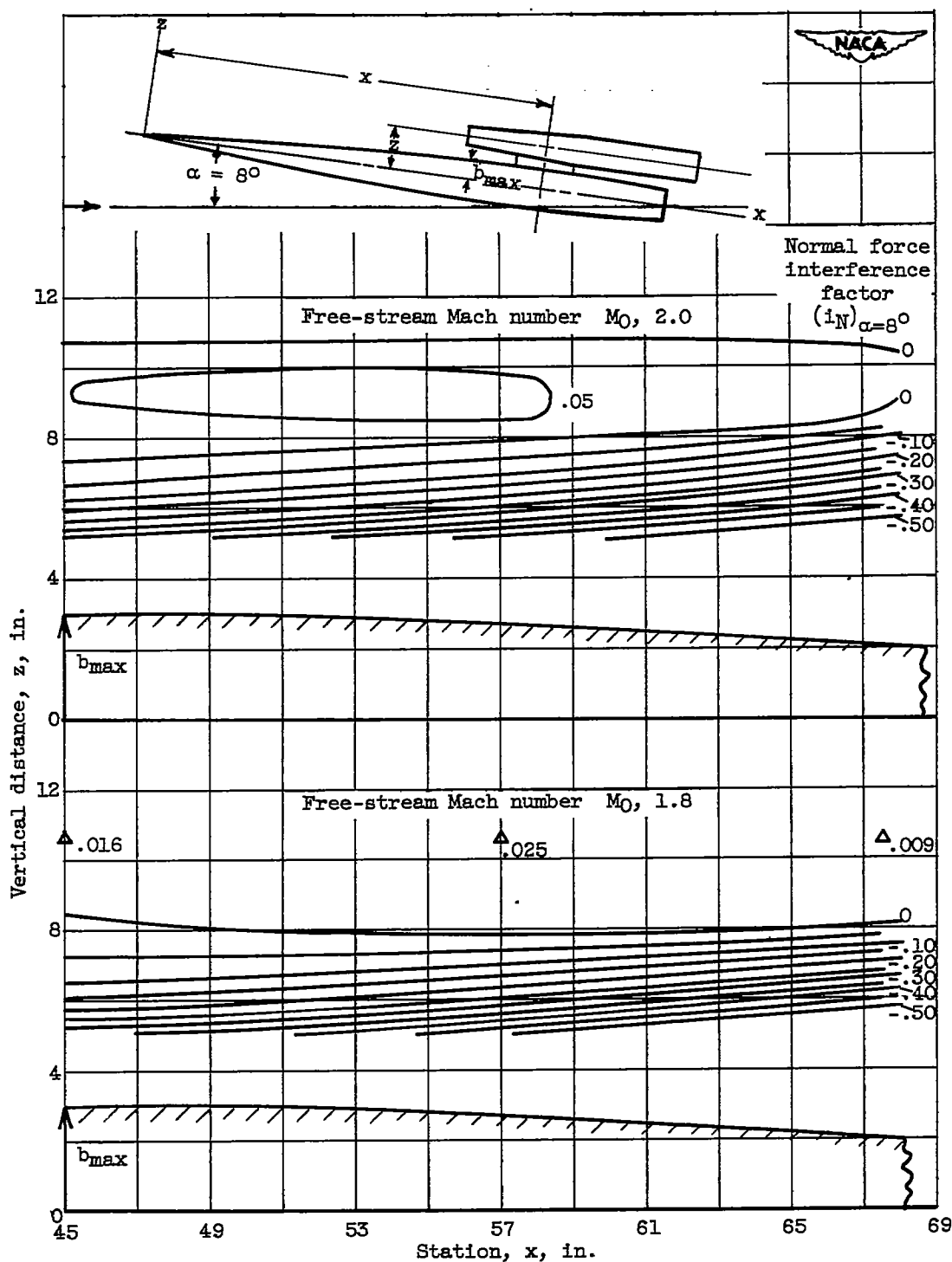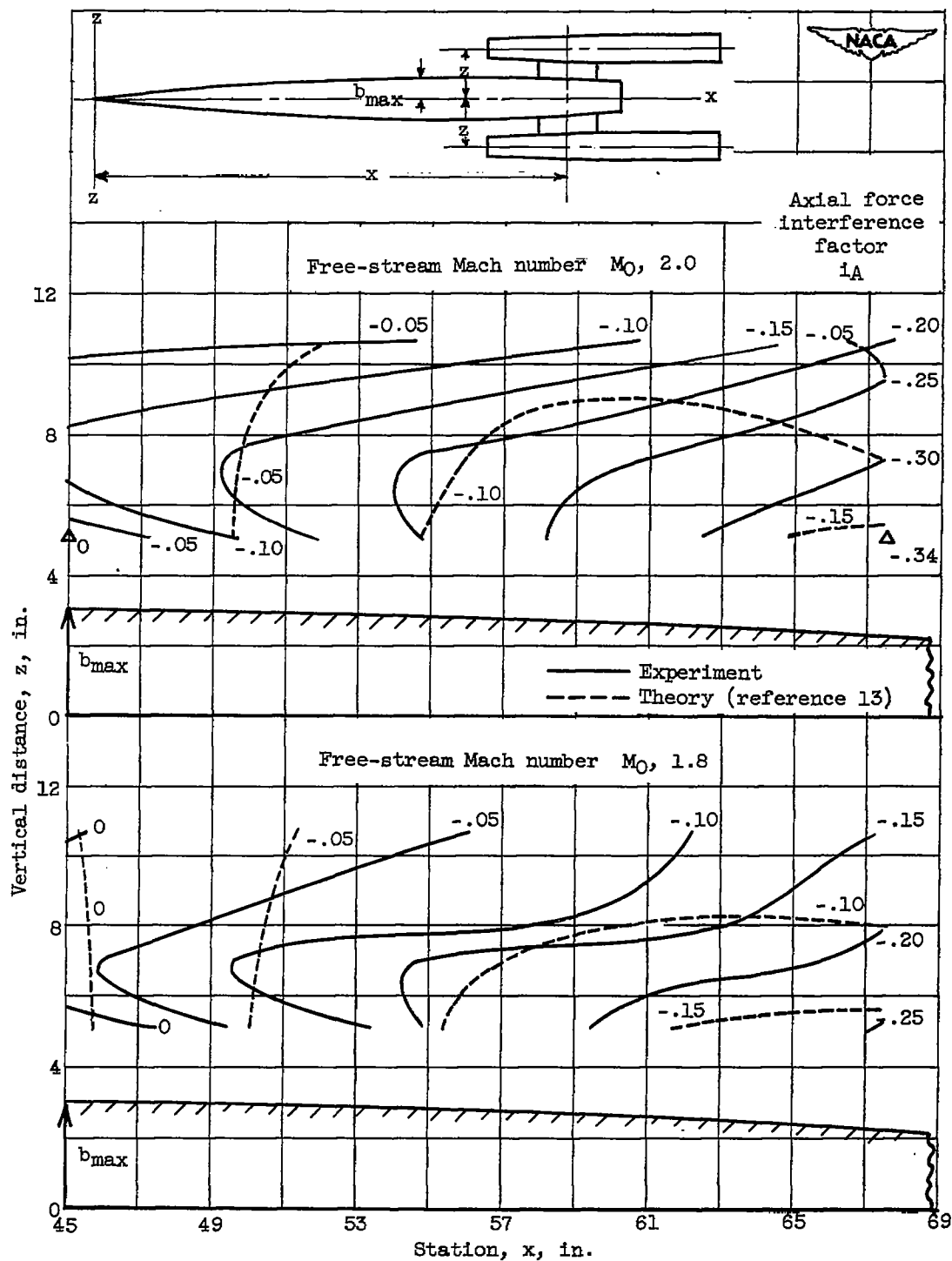(b) Lower-engine configurations.

Figure 5. - Continued. Contours of normal force interference factor. Angle of attack, 2°.
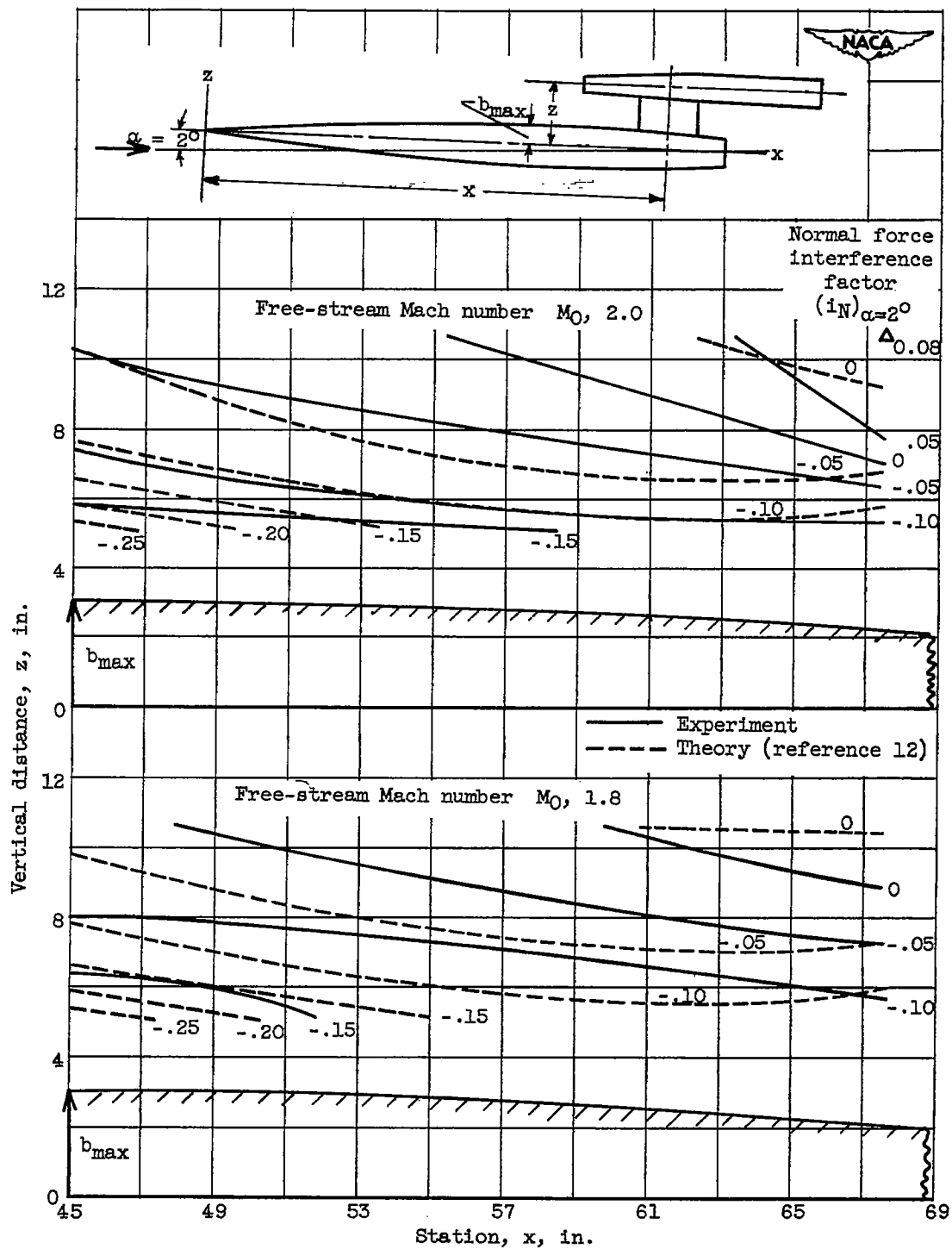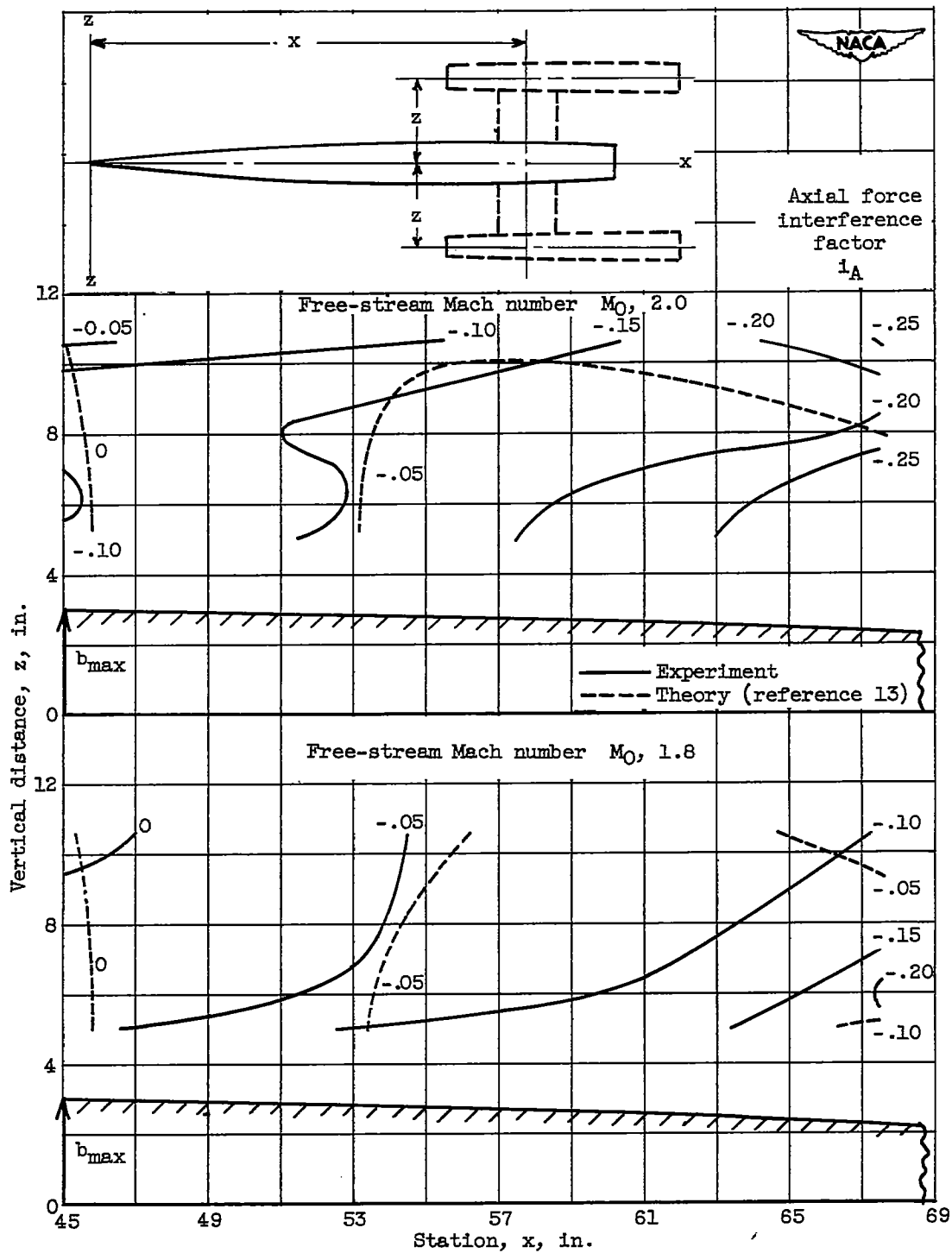
(c) Upper-engine configurations.

Figure 5. - Concluded.   Contours of normal force interference factor. Angle of attack, 2°.

2438
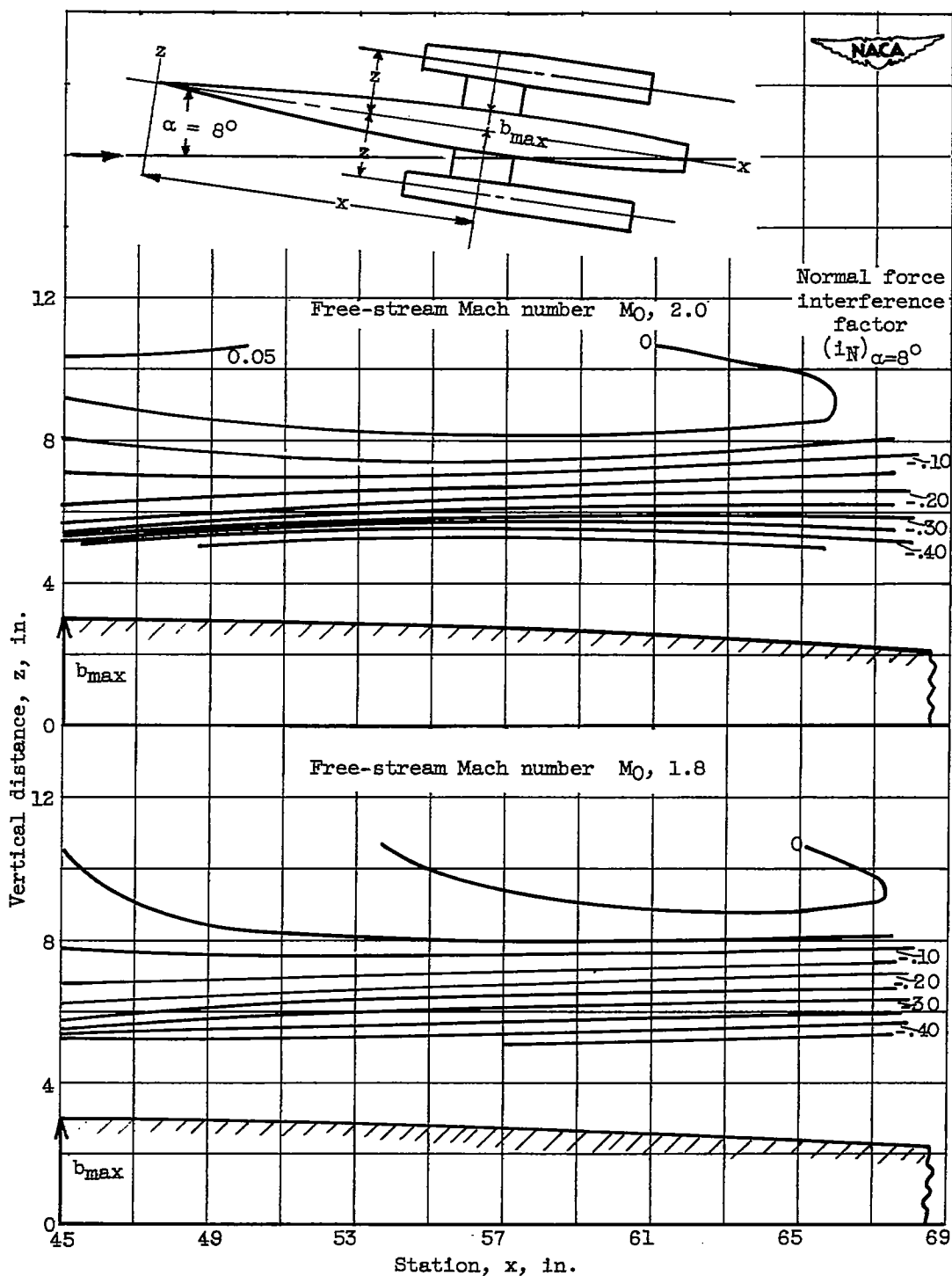
(a) Twin-engine configurations.

Figure 6. - Contours of normal force interference factor. Angle of attack, $8°$.

(b) Lower-engine configurations.

Figure 6. - Continued.   Contours of normal force interference factor.   Angle of attack, 8°.

(c) Upper-engine configurations.

Figure 6. - Concluded. Contours of normal force interference factor. Angle of attack, 8°.

(a) Twin-engine configurations.

Figure 7. - Contours of axial force interference factor. Angle of attack, 0°.

(b) Single-engine configurations.

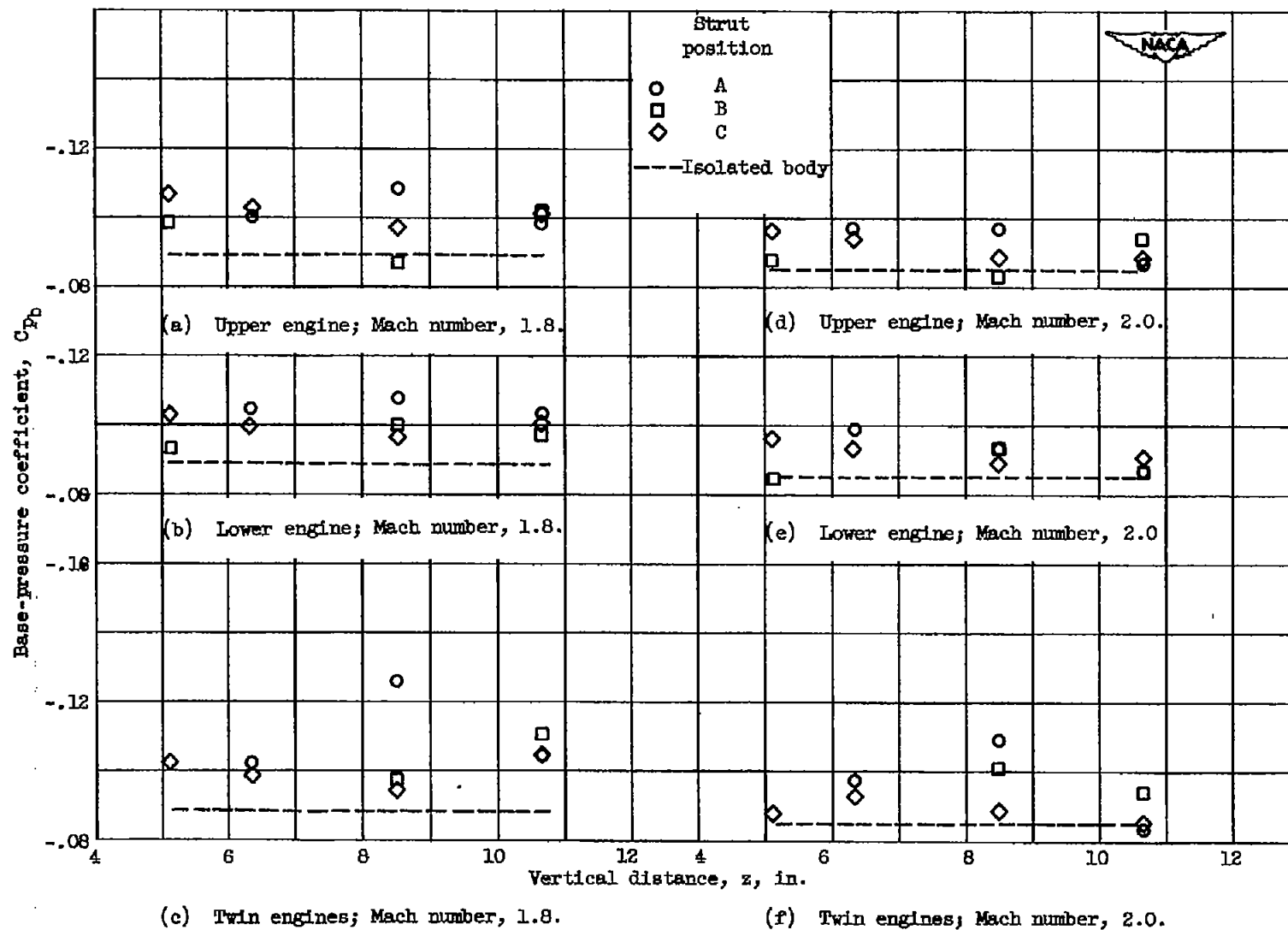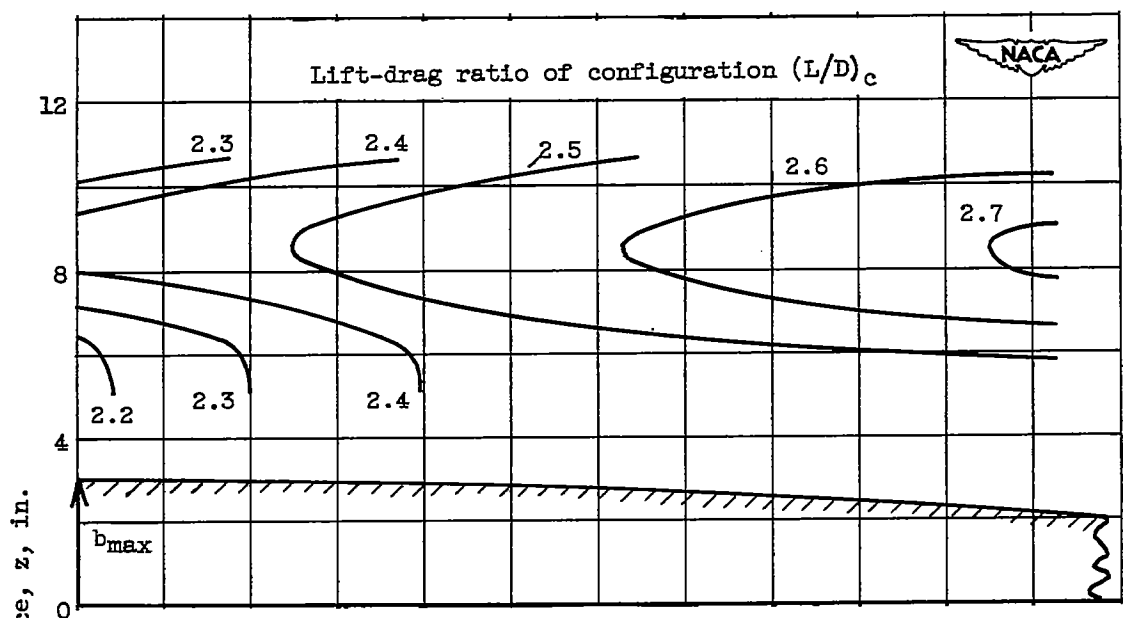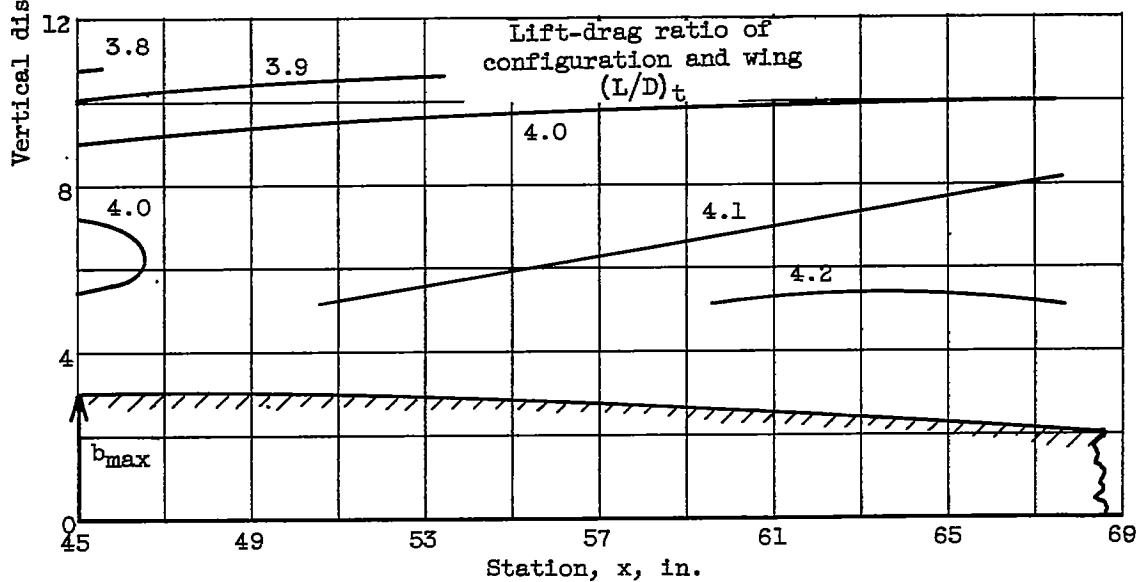Figure 7. - Concluded. Contours of axial force interference factor. Angle of attack, 0°.

Figure 8. - Body base-pressure coefficient as function of strut length. Angle of attack, 0°.

(a) Upper engine; Mach number, 1.8.

(b) Lower engine; Mach number, 1.8.

(c) Twin engines; Mach number, 1.8.

(d) Upper engine; Mach number, 2.0.

(e) Lower engine; Mach number, 2.0

(f) Twin engines; Mach number, 2.0.

(a) Configurations alone.

(b) Configurations with wing.

Figure 9. - Contours of lift-drag ratio for twin-engine configurations. Mach
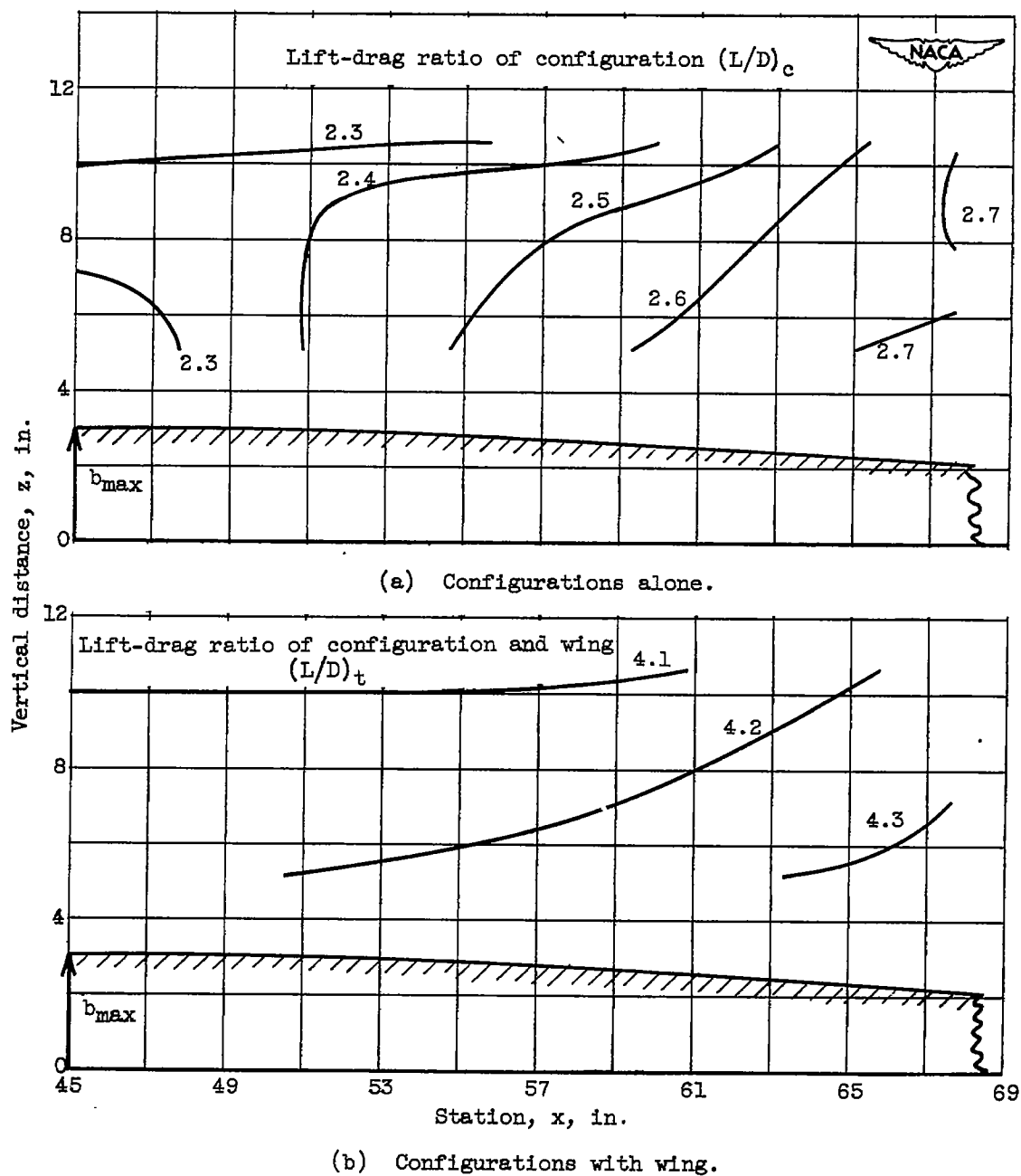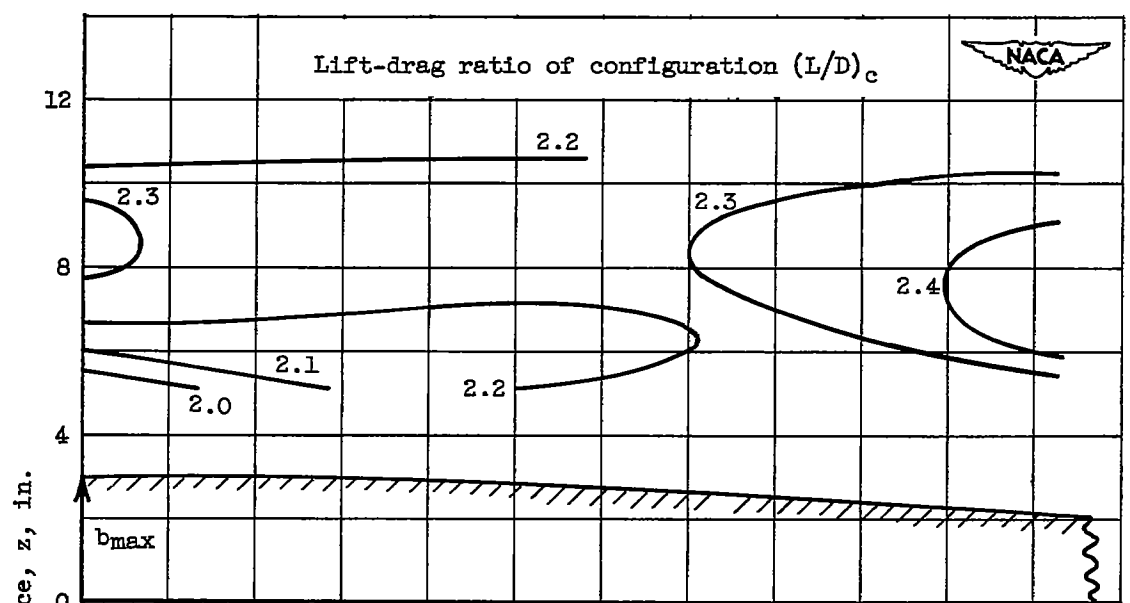number, 2.0; angle of attack of configuration, 8°; lift-drag ratio of wing,
5.0.

Lift-drag ratio of configuration $(L/D)_c$

2.3

2.4

2.5

2.7

2.6

2.3

2.7

b_{max}

(a)   Configurations alone.

Lift-drag ratio of configuration and wing $(L/D)_t$

4.1

4.2

4.3

b_{max}

| 45 | 49 | 53 | 57 | 61 | 65 | 69 |

Station, x, in.

(b)   Configurations with wing.

Figure 10. - Contours of lift-drag ratio for lower-engine configurations. Mach number, 2.0; angle of attack of configuration, 8°; lift-drag ratio of wing, 5.0.
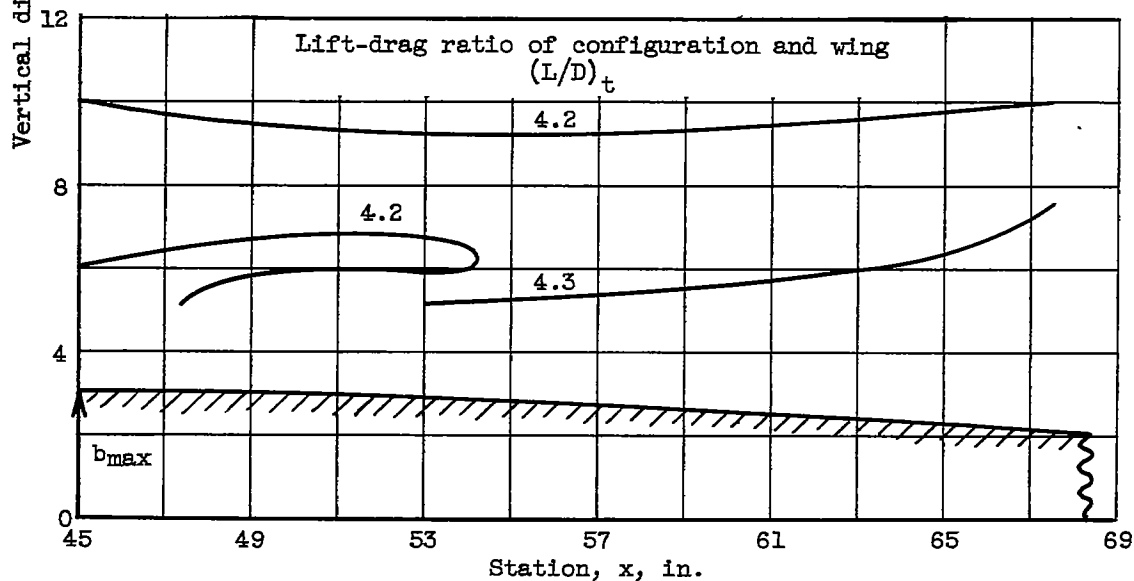
Vertical distance, z, in.

(a)   Configurations alone.

(b)   Configurations with wing.

Figure 11. - Contours of lift-drag ratio for upper-engine configurations. Mach
number, 2.0; angle of attack of configuration, 8°; lift-drag ratio of wing,
5.0.